29. Minimum temperature data for the United States and Japan and snowfall data for the United State are based on station data. Daily minimum temperature data for Paris, Novosibirsk, and Beijing were derived using 6-hourly data from the NCEP/NCAR Reanalysis, and snowfall data for Paris and Tokyo were derived from the NCEP/NCAR Reanalysis as precipitation days when the daily mean temperature was below 0°C.

30. Buoy 46005 (located off the coast of Washington State at 46°N, 131°W) and Buoy 44005 (located off the coast of New England at 43°N, 69°W). Winds are based on station data.

31. Blocking events are defined as intervals in which 500-hPa height from the NCEP/NCAR Reanalysis exceeds 1 SD about its mean for five consecutive days. The regions listed in Table 2 correspond to those regions where high-latitude blocking is observed to occur most frequently [J. Shukla, K. Mo, *Mon. Weather Rev.* **111**, 388 (1983)].

32. Thanks to M. P. Baldwin, C. S. Bretherton, C. Deser, D. L. Hartmann, M. Hiltner, M. Holmberg, J. Hurrell, N. J. Mantua, and C. F. Mass for their help at various stages of this research and also to the anonymous reviewers for their insightful comments. D.W.J.T. was supported by the NASA Earth System Science Fellowship Program and by funding provided through Colorado State University. J.M.W. was supported by the NSF under Grant 9707069.

Seasonal Modulation of Interseismic Strain Buildup in Northeastern Japan Driven by Snow Loads

Kosuke Heki

Distinct periodic variations with annual frequencies are often found in the time series of continuous Global Positioning System (GPS) site coordinates in northeastern Japan. They show maximum arc-normal contraction of a few millimeters as well as maximum subsidence of 1 to 2 centimeters, both in March. In northeastern Japan, it snows heavily on the western flank of the backbone range, attaining a maximum depth of several meters in March. When observed snow depths were compared with the load distribution estimated from the GPS data, the surface loads caused by the snow were found to be largely responsible for the annual displacement of GPS sites. The snow load modulates secular strain buildup in northeastern Japan due to the Pacific Plate subduction, but its relevance to the seasonal change of earthquake occurrences remains uncertain.

The GPS Earth Observation Network (GEO-NET), the nationwide continuous GPS array run by the Geographical Survey Institute (GSI), Japan, has been useful as a sensor for secular (*1*) and earthquake-specific (*2, 3*) crustal deformation. These GPS site coordinates often show conspicuous seasonal variations in addition to interseismic secular movements. Recently, Murakami and Miyazaki (*4*) found that the seasonal signals are coherent in phase to a large extent, and their amplitudes are systematic in space. They fixed a station in central Japan (Komatsu, Fig. 1) and showed that the directions of the annual signals relative to Komatsu coincide with the plate convergence at the Japan Trench, and that their amplitudes are larger where secular velocities are faster. These features suggest an unforeseen possibility that the plate velocity or the coupling strength at depth changes annually (i.e., faster subduction or stronger coupling occurs in winter).

Murakami and Miyazaki (*4*) confirmed that the annual signals are consistent for different receiver and antenna types, and for solutions with different software packages with and without the estimation of atmospheric delay gradients (*5*). They further con-

firmed that similar annual signals exist in the data from the Japanese domestic very long baseline interferometry (VLBI) observations (*6*). Thus, despite the lack of physical explanation for the seasonal variations, they suggested that the signals are real. Here, I investigated whether snow accumulation in northeastern Japan can provide a sufficient surface load to reproduce the necessary elastic deformation of the solid Earth to account for the GPS variations. Such a finding would thus serve as an independent confirmation of the reality of the signal.

Daily solutions of the GEONET GPS site coordinates relative to the central station at Tsukuba, Ibaraki (Fig. 1), were taken from the GSI website (www.gsi.go.jp) for northeastern Japan covering the period 1998.9–2001.0. The data are based on a routine analysis strategy (*7*) of GSI and are essentially of the same quality as the 1996–1999 data used by Murakami and Miyazaki (*4*). They fixed the Komatsu station (Fig. 1) because its secular velocity represents that of the Eurasian Plate. Here, however, I considered pairs of GPS points that represent the western and eastern sides of the island arc, and compared their baseline length time series.

The baselines on the Japan Sea side have large annual components: They shorten by a few millimeters in winter (Fig. 2, B and E), a result consistent with (*4*). On the other hand,

seasonal signatures are smaller on the Pacific side of the arc (Fig. 2, A and D) and have the opposite sense (shortening in summer). Such a contrast across the backbone range is seen for most pairs of baselines. If the annual signal reflects changes in the convergence rate or the coupling strength at the Japan Trench, its amplitude would be proportional to the secular shortening rate, irrespective of which side of the arc the baseline lies. Another feature not mentioned in (*4*) is the annual signals in vertical components (Fig. 2, C and F). Most of the sites subside relative to Tsukuba in the winter, and the amplitudes, up to ~2 cm peak-to-peak, are larger along the backbone range than along the coasts. Neither faster subduction nor stronger coupling predicts such a subsidence pattern for the arc. These features make the trench-origin mechanisms untenable.

Four seasons characterize the environment in Japan. In winter, cold and dry air over Siberia becomes humid as it travels across the Japan Sea, leaving heavy snowfalls as it collides with the backbone range of northeastern Japan. Snow mainly falls on the western side of the arc, but the amounts vary from place to place. The deepest snow, seen along the western flank of the backbone range, starts to accumulate in late autumn, reaching a few meters deep in March; it then disappears in May (Fig. 1) except at the highest peaks. Loads on Earth's surface cause subsidence beneath and around these peaks, along with horizontal deformation such that the land shortens beneath the load and extends outside of it. Snow loads distributed along the western half of the arc would cause crustal deformation qualitatively consistent with the GPS baseline data (Fig. 2), arc-normal crustal shortening beneath the snow cover (Fig. 2, B and E), and smaller extension outside the cover (Fig. 2, A and D). It would also cause the subsidence whose maximum lies below the snow load center (Fig. 2, C and F).

Next, I fixed an arbitrary station and modeled each component of the relative position time series of 88 GPS points in northeastern Japan with the linear, annual, and biannual terms (*8*). I discarded 13 sites (*9*) whose root mean squares of the post-fit residuals exceeded 4 mm (horizontal) or 15 mm (vertical). Then I obtained instanta-

Division of Earth Rotation, National Astronomical Observatory, 2-12 Hoshigaoka, Mizusawa, Iwate 023-0861, Japan. E-mail: heki@miz.nao.ac.jp
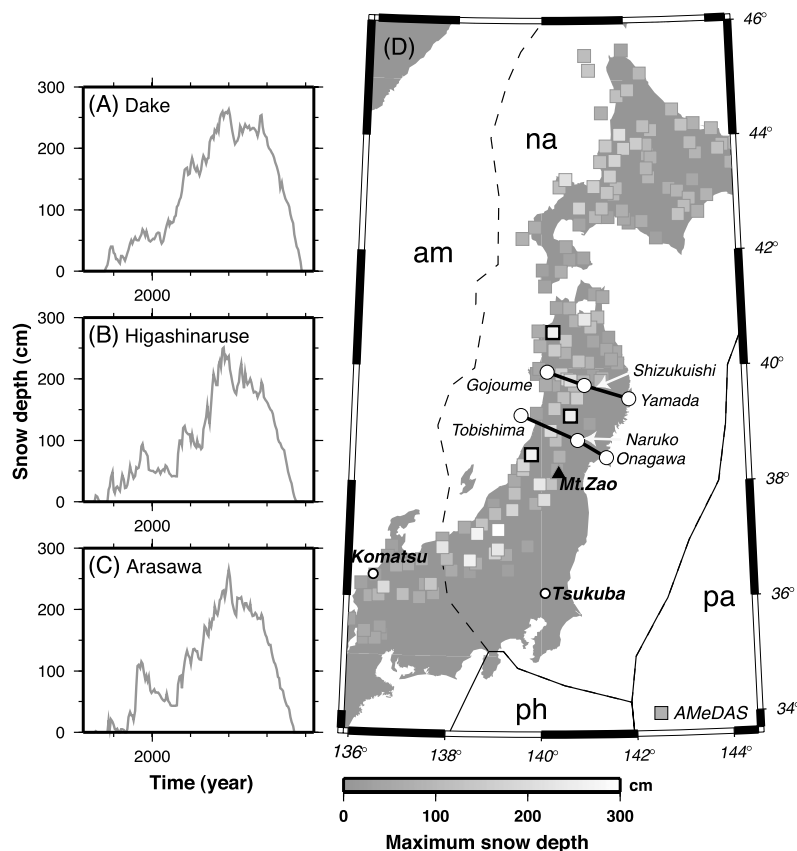
Fig. 1. (**A** to **C**) Time series of snow depth during the 1999–2000 winter season at three points shown in (**D**) by squares drawn with bold lines (tick marks in the horizontal axes show months). Other squares in (D) show the maximum snow depths in the 1999–2000 winter obtained at the AMeDAS sites (*13*). Only sites with maximum depths of >30 cm are plotted. In (D), tectonic plates and their boundaries are shown [na, North American Plate; am, Amurian Plate (*23*); pa, Pacific Plate; ph, Philippine Sea Plate]; lines connecting the white circles are the baselines whose changes in lengths are plotted in Fig. 2.
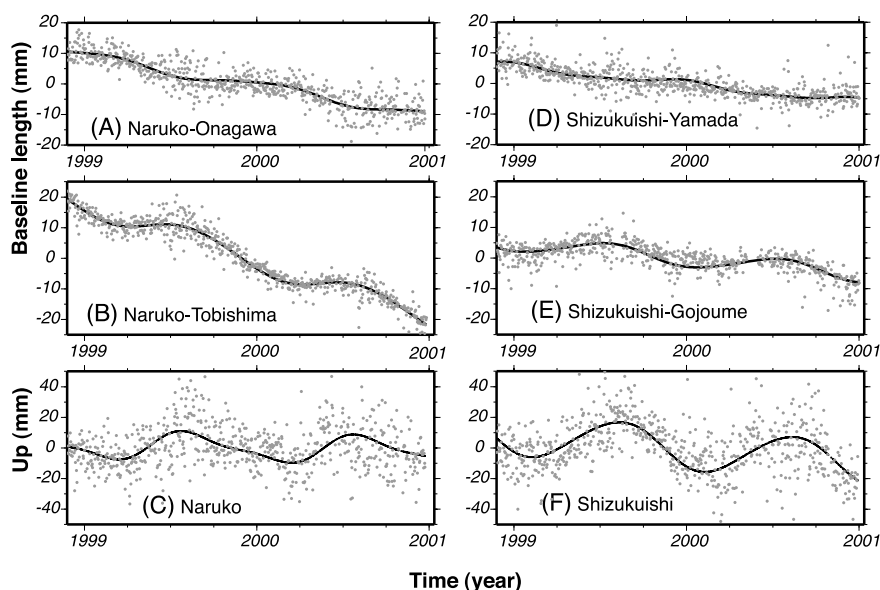

Fig. 2. Time series, covering the period 1998.9–2001, of the baseline lengths on the eastern (**A** and **D**) and the western (**B** and **E**) sides of northeastern Japan. (**C** and **F**) Vertical position of the Naruko and Shizukuishi stations, respectively, relative to Tsukuba, Ibaraki, far to the south (Fig. 1D). Gray dots show daily solutions; solid curves are best-fit lines assuming periodic (annual and biannual) and linear changes.

neous values of the periodic components on 15 March (relative to 15 August) for all the sites (Fig. 3) and estimated the load (heights of the water columns above ground) on each of the rectangular areas as large as 0.5° in latitude and 0.75° in longitude covering the land area in Fig. 3 that best explained the observed winter-summer site displacements in a least-squares sense (*10*). I simultaneously estimated the translation of the whole network to ensure that the obtained loads were free from the fixed-point problem. To calculate site displacements due to a unit load on an elastic half-space, I used the formulation by Farrel (*11*), 30 GPa for rigidity, and 0.25 for Poisson's ratio. Typical formal errors of the estimated load were around 20 to 25 cm, and the post-fit residuals of the input data were 1.3 mm, 0.9 mm, and 2.9 mm for the north, east, and up components, respectively.

In Fig. 3, some stations have anomalously large residuals, a part of which might be explained by localized high snow masses often found over the high mountains. Nonetheless, the observations agree with the calculated displacements. To convert the load into snow depth, I needed data for average snow density, which can be obtained only by field observations of snow cross sections. Such observations have been carried out at Mount Zao (Fig. 1D), and Yamaya *et al.* (*12*) report that the average snow densities there during the 1999–2000 winter increased with time (i.e., 0.30 to 0.32 g/cm³ from January to February, 0.42 g/cm³ in late March, and 0.50 to 0.53 g/cm³ from the end of April to May).

I assumed a snow density of 0.4 g/cm³ in the middle of March to convert the load into snow depth, and compared the resulting estimates with snow depth data acquired on 15 March 2000 at AMeDAS (Automated Meteorological Data Acquisition System) stations (*13*) (Fig. 4). The data sets were fairly consistent (*14*), which suggested that the snow could explain most of the annual GPS variations. Other hydrological factors (e.g., soil moisture and groundwater) would be less important, but they would reduce the sharpness of the load decrease by spring thawing. Atmospheric pressure increase in winter [~1 kPa (*15*) in northeastern Japan] would act as the equivalent of additional snow as deep as 25 cm for the entire land area and would enhance the annual signature by ~10%. Snow covers are ubiquitous in high- to mid-latitude areas on Earth. Snow loads, together with various water-loading mechanisms (*16*), would annually distort the terrestrial reference frame composed of worldwide distributed stations. This would substantially affect the determination of GPS orbits because the current accuracy of the terrestrial reference frame is ~1 cm or better (*17*). (Here I discuss relative displacements within a local net-
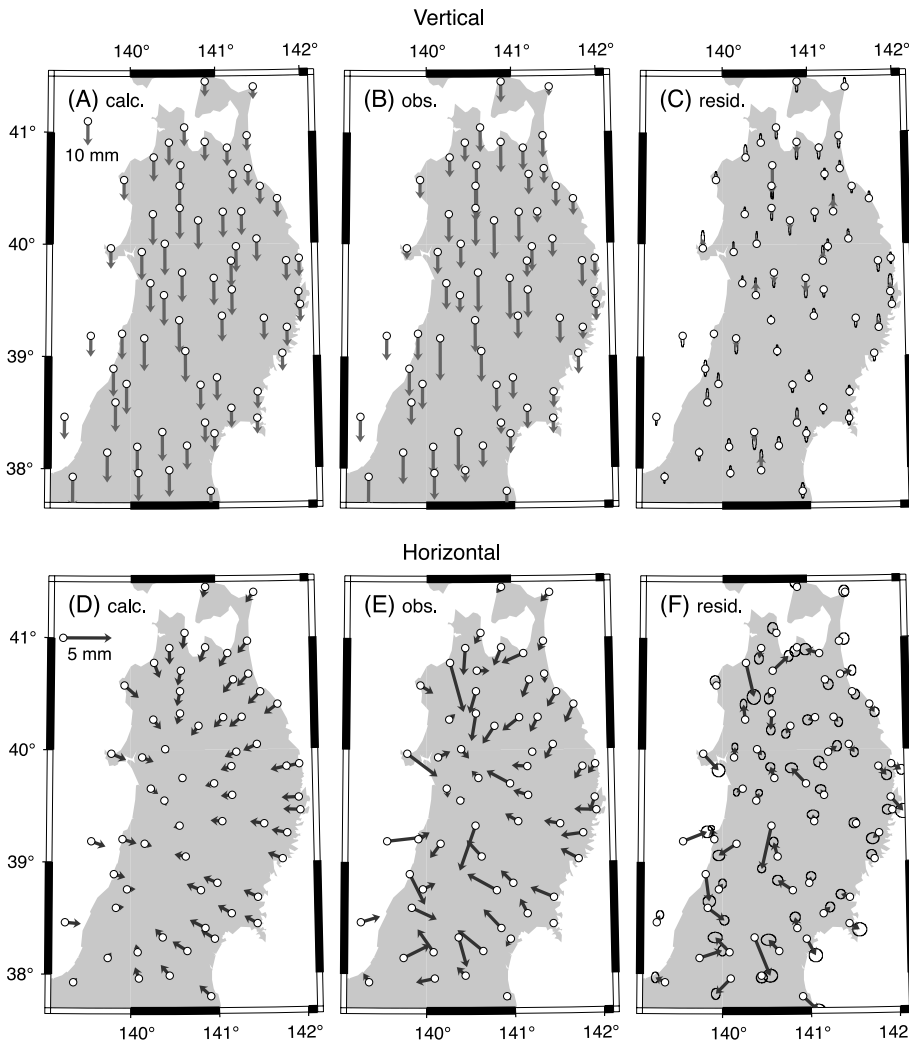
Fig. 3. Values of the periodic terms of the vertical (**A** to **C**) and horizontal (**D** to **F**) coordinates on 15 March relative to 15 August (B and E), those calculated from the estimated load distribution (A and D), and their differences (C and F). Error ellipses attached to the residual vectors show 1σ uncertainties of the observed vectors. Translation of the whole network, estimated together with loads, is added to the observed vectors to make them absolute.

Fig. 4. (**A**) Snow depth data at the AMeDAS (*13*) sites on the middle day of March 2000. (**B**) Snow depths converted from the loads estimated by the GPS data. The average snow density was assumed to be 0.4 g/cm³.

let us conclude that there is a causal relation between earthquakes and the snow loads, even if we took into account that the earthquake-triggering mechanisms are not well understood.

References and Notes
1. S. Miyazaki, K. Heki, *J. Geophys. Res.* **106**, 4305 (2001).
2. H. Tsuji, Y. Hatanaka, T. Sagiya, M. Hashimoto, *Geophys. Res. Lett.* **22**, 1669 (1995).
3. K. Heki, S. Miyazaki, H. Tsuji, *Nature* **386**, 595 (1997).
4. M. Murakami, M. S. Miyazaki, *Geophys. Res. Lett.*, in press.
5. D. S. MacMillan, *Geophys. Res. Lett.* **22**, 1041 (1995).
6. R. Ichikawa *et al.*, paper presented at the Third Joint Meeting of U.S.-Japan Natural Resources Panel on Earthquake Research, November 2000.
7. S. Miyazaki, T. Saito, M. Sasaki, Y. Hatanaka, Y. Iimura, *Bull. Geog. Surv. Inst.* **43**, 23 (1997).
8. The annual variation curve is asymmetric about the peak. For example, the subsidence in winter is somewhat slower than the uplift in spring (Fig. 2, C and F), which can be modeled by combining annually and biannually changing terms. It was also confirmed that the results are not dependent on the particular station chosen as the fixed point.
9. The discarded stations mostly belong to the first-generation GPS points (established in 1994) of GEONET and do not concentrate on a particular area. They had larger post-fit residuals than the newer points.
10. A weak continuity constraint was imposed to stabilize the solution so that the difference of the loads of the adjacent rectangles is 0 ± 20 cm (or ±50 cm for the depth of snow as dense as 0.4 g/cm³).
11. W. E. Farrel, *Rev. Geophys. Space Phys.* **10**, 761 (1972).
12. M. Yamaya *et al.*, *Tohoku J. Natural Disaster Sci.* **36**, 171 (2000).
13. *Monthly Rep. Jpn. Meteorol. Agency* **3**, no. 5 (2000).
14. Because AMeDAS stations need public electricity and communication lines, they are generally located in inhabited lowlands. This may have negatively biased observed snow depths and would partly explain the apparent absence of snow on the Pacific side in Fig. 4A.

work, which are little affected by such errors, but annual variations in global GPS networks are more sensitive to the annual orbital errors and need to be examined carefully.)

The snow loads modulate interseismic stress buildup in northeastern Japan (Fig. 2, B and E). Seasonality in earthquake occurrences is a century-long issue (*18*) in Japanese seismology, and Murakami and Miyazaki (*4*) suggested the relevance of the seasonal strain changes to the seismicity. Mogi (*19*) compiled historical ($M \geq 7.9$) and modern ($M \geq 7.5$) earthquakes, and found that the peak in seismicity exists in March in northeastern Japan and in December in central Japan. Ohtake and Nakahara (*20*) confirmed the statistical significance of the seasonality in central Japan and evaluated its relevance to the atmospheric pressure increase of ~1 kPa in winter. They showed that this high pressure qualitatively encourages reverse slips at the plate interface, but the

stress changes are only a few tens of Pa in terms of the Coulomb failure function (CFF) (*21*). This is not larger than the semidiurnal tidal stress increase of up to ~1 kPa, which is not effective in triggering earthquakes (*21*).

Recently, Gao *et al.* (*22*) suggested that the higher activity of the 1992 Landers event aftershocks in summer might be due to the atmospheric pressure change of ~2 kPa, which is an order of magnitude smaller than the minimum static stress changes previously considered to trigger aftershocks. The snow loads inferred in the present study are equivalent to an increase of up to ~10 kPa in atmospheric load, and a calculation similar to that in (*20*) shows that they cause positive CFF change at the plate interface dipping westward from the Japan Trench (Fig. 1). However, the same calculation also indicates that the large distance between the load and the fault reduces the CFF change down to the level of 0.1 kPa. This would be too small to
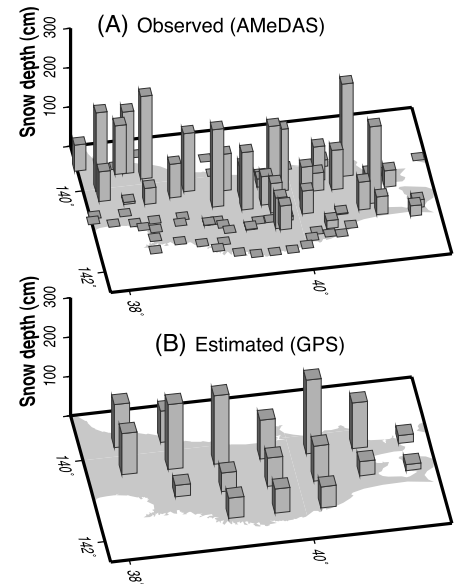
15. National Astronomical Observatory (Ed.), *Chronological Scientific Tables 74* (Maruzen, Tokyo, 2000).
16. T. van Dam *et al.*, *Geophys. Res. Lett.* **28**, 651 (2001).
17. P. Sillard, Z. Altamimi, C. Boucher, *Geophys. Res. Lett.* **25**, 3223 (1998).
18. F. Omori, *Pub. Earthq. Invest. Comm.* **8**, 1 (1902).
19. K. Mogi, *Bull. Earthq. Res. Inst.* **47**, 419 (1969).
20. M. Ohtake, H. Nakahara, *Pure Appl. Geophys.* **155**, 689 (1999).
21. R. S. Stein, *Nature* **402**, 605 (1999).
22. S. S. Gao, P. G. Silver, A. T. Linde, I. S. Sacks, *Nature* **406**, 500 (2000).
23. K. Heki *et al.*, *J. Geophys. Res.* **104**, 29147 (1999).
24. I thank M. Murakami, who first reminded me of the geophysical importance of the annual signals; T. Iwabuchi for providing AMeDAS snow depth data; and S. Miyazaki for reviewing the earlier version of the manuscript.

Massive Expansion of Marine Archaea During a Mid-Cretaceous Oceanic Anoxic Event

Marcel M. M. Kuypers,[1]* Peter Blokker,[1]† Jochen Erbacher,[2] Hanno Kinkel,[1] Richard D. Pancost,[1]‡ Stefan Schouten,[1] Jaap S. Sinninghe Damsté[1]§

Biogeochemical and stable carbon isotopic analysis of black-shale sequences deposited during an Albian oceanic anoxic event ($\sim$112 million years ago) indicate that up to 80 weight percent of sedimentary organic carbon is derived from marine, nonthermophilic archaea. The carbon-13 content of archaeal molecular fossils indicates that these archaea were living chemoautotrophically. Their massive expansion may have been a response to the strong stratification of the ocean during this anoxic event. Indeed, the sedimentary record of archaeal membrane lipids suggests that this anoxic event marks a time in Earth history at which certain hyperthermophilic archaea adapted to low-temperature environments.

The mid-Cretaceous was a period of exceptional oceanic volcanic activity. Evidence of this igneous activity is provided by the presence of large oceanic plateaus, including the Ontong Java, Kerguelen, and Caribbean Plateau, which have been dated at 125 to 88 million years (*1*). Enhanced volcanic outgassing of CO_2 could have caused the mid-Cretaceous "greenhouse" climate (*2*), with its minimal equator-to-pole temperature difference. In contrast, episodic oceanic anoxic events (OAEs) may have effectively reduced CO_2 concentrations during brief periods by

sequestering carbon in the subsurface (*3*, *4*). The widespread deposition of black shales during the OAEs has been attributed either to decreased organic matter (OM) remineralization resulting from a decreased oxygen flux (*5*) or to increased primary productivity overwhelming the oxic OM remineralization potential of the water column (*6*). The increase in organic carbon (OC) accumulation rates during the OAEs in these two basically different models is attributed to enhanced burial of marine OM, which is typically of phytoplanktonic origin. Here we determined the source for both soluble and insoluble OM of the early Albian OAE1b black shales of the Ocean Drilling Program site 1049C (North Atlantic Ocean off the coast of Florida: 30°08′N, 76°06′W) and the Ravel section of the Southeast France Basin (44°06′N, 6°28′E) using optical, chemical, and stable carbon isotopic analyses and show that the sources of OM for this OAE are fundamentally different from those of other OAEs.

The upper Aptian–lower Albian sequence of site 1049C consists of marls and calcareous marls characterized by a low (<0.1 weight %) (wt %) OC content interrupted by an OC-rich (up to 6 wt %) (Fig. 1A) black-shale interval. This black-shale interval

(Fig. 1) has been identified as the local expression of OAE1b (*7*). The bulk OC shows a sharp increase in ^{13}C content during the OAE1b (Fig. 1B). Similar increases in ^{13}C isotopic ($\delta^{13}C$) values observed for marine carbonates and OM from other mid-Cretaceous OAEs have been attributed to an increase in the ^{13}C content of the oceanic and atmospheric pool of inorganic carbon as a result of globally enhanced OC burial rates (*3*). However, the stable carbon isotopic composition of picked planktonic and benthic foraminifers (*7*) indicates that there was no substantial increase in $\delta^{13}C$ values for inorganic carbon during the OAE1b at site 1049C.

To resolve the origin of the increase in $\delta^{13}C$ values for bulk OC ($\delta^{13}C_{org.}$), we first analyzed the extractable OM. The saturated hydrocarbon fractions of the black shales contain long-chain (C_{25} to C_{31}) *n*-alkanes that are largely derived from leaf waxes of terrestrial plants, some bacterial hopanoids, and acyclic isoprenoids. Unexpectedly, the acyclic isoprenoid, 2,6,15,19-tetramethylicosane [TMI (**I**), Fig. 1] is the most abundant component of the saturated hydrocarbon fraction. So far, TMI has been found only in the contemporaneous (*7*) OAE1b black shale of the Ravel section in France (*8*). TMI (**I**) is structurally closely related to 2,6,10,15,19-pentamethylicosane (PMI) (**II**), a compound of known archaeal origin (*9*), which was also present in the saturated hydrocarbon fraction. Further evidence for archaeal compounds was found on treating the polar fraction from the black-shale interval with $HI/LiAlH_4$ to cleave ether bonds. The released fractions were dominated by acyclic (**a**), monocyclic (**b**), bicyclic (**c**), and tricyclic (**d**) biphytanes (C_{40} isoprenoids), which are also exclusively found in archaea (*10*, *11*). In addition, a recently developed high-performance liquid chromatography–mass spectrometry (HPLC-MS) technique (*12*) revealed the presence of four (**III** to **VI**) intact isoprenoid glycerol dialkyl glycerol tetraethers (GDGTs) in the black-shale interval. GDGTs are the main constituents of archaeal membranes (*11*), and **IV** and **V** are characteristic of the archaeal lineage Crenarchaeota (*10*, *13*), which includes the hyperthermophilic archaea that thrive at temperatures >60°C. In contrast, **VI** is highly diagnostic of their nonthermophilic relatives (*11*, *14–16*), and the dominance of this compound (representing 60% of total GDGTs) indicates an important contribution of nonthermophilic crenarchaeota. To the best of our knowledge, this is the earliest fossil evidence for marine nonhyperthermophilic crenarchaeota, extending their geological record by more than 60 million years (*14*).

The $\delta^{13}C$ values of components of unambiguous archaeal origin such as **II**, **c**, and **d** and the related **I** are substantially enriched in ^{13}C relative to algal steroids **VII** and **VIII** (Fig. 1, C and D), bacterial-

[1]Department of Marine Biogeochemistry and Toxicology, Netherlands Institute for Sea Research (NIOZ), Post Office Box 59, 1790 AB Den Burg, Netherlands. [2]Referat Meeresgeologie, Bundesanstalt für Geowissenschaften und Rohstoffe, Stilleweg 2, 30655 Hannover, Germany.

*Present address: Department of Biogeochemsitry, Max Planck Institute for Marine Microbiology, Celciusstrasse 1, Bremen, 28359 Germany.
†Present address: Department of Analytical and Applied Spectroscopy, Vrije Universiteit, De Boelelaan 1083, 1081 HV Amsterdam, Netherlands.
‡Present address: Organic Geochemistry Unit, School of Chemistry, University of Bristol, Cantock's Close, Bristol BS8 1TS, UK.
§To whom correspondence should be addressed. E-mail: damste@nioz.nl